

SHOCK-HEATED NH₃ IN A MOLECULAR JET ASSOCIATED WITH A HIGH-MASS YOUNG STAR

QIZHOU ZHANG,¹ TODD R. HUNTER,¹ T. K. SRIDHARAN,^{1,2} AND RICCARDO CESARONI³

Received 1999 September 24; accepted 1999 October 26; published 1999 November 29

ABSTRACT

We present the discovery of shock-excited NH₃ in a well-collimated jet associated with the extremely young high-mass star IRAS 20126+4104. The NH₃ (3, 3) and (4, 4) emission is dominated by three clumps along the SiO jet. At the end of the jet, there exists strong and broad (± 10 km s⁻¹) NH₃ (3, 3) emission. With typical brightness temperatures greater than 500 K, the overall emission indicates a weakly inverted population and appears in an arc, consistent with the excitation by bow shocks. There are two bright spots in the NH₃ (3, 3) emission with brightness temperatures of approximately 2000 K. The narrow line width (1.5 km s⁻¹ FWHM), the small sizes ($<0\prime.3$), and the unusually high brightness temperature of the features are indicative of maser emission. Our observations provide clear evidence that NH₃ (3, 3) masers are excited in shock regions in molecular outflows.

Subject headings: H II regions — ISM: clouds — ISM: individual (IRAS 20126+4104) —
ISM: kinematics and dynamics — masers — stars: formation — stars: pre-main-sequence

1. INTRODUCTION

IRAS 20126+4106 is a young star lying in the Cygnus X complex at a distance of 1.7 kpc (Wilking et al. 1989). Its luminosity of $1.3 \times 10^4 L_{\odot}$ corresponds to a zero-age main-sequence star of spectral type B0.2. Despite the high luminosity, sensitive observations with the VLA have failed to detect a radio continuum counterpart until recently. Recent VLA-B observations resolved the 3.6 cm continuum source into an elongated structure (Hofner et al. 1999). In conjunction with upper limits at other wavelengths, Hofner et al. interpreted this source as emission from an ionized jet. The lack of a detectable H II region indicates that the central object is probably a high-mass protostar. In contrast to the weak centimeter emission, the source is detected at all wavelengths in the millimeter to sub-millimeter bands (Cesaroni et al. 1999). Its spectral energy distribution is consistent with optically thin dust emission with an emissivity index of $\beta = 1$.

One of the most interesting aspects of the source came from the spectral line studies: Both the CH₃CN (Cesaroni et al. 1997, 1999) and the NH₃ (1, 1) and (2, 2) lines (Zhang, Hunter, & Sridharan 1998) show an elongated disklike structure perpendicular to the narrow SiO jet and the HCO⁺ outflow (Cesaroni et al. 1997, 1999). The velocity field in the disk is consistent with Keplerian rotation. Although the CO outflow mapped in the (2–1) transition extends more than 1 pc in the north-south direction, the CO (7–6) outflow (Kawamura et al. 1999) is compact (<0.1 pc), with an orientation and size consistent with the SiO jet and the HCO⁺ outflow.

IRAS 20126+4104 is one of the rare examples of a disk/jet system surrounding a high-mass young star. It clearly demonstrates that disks are involved in the formation of high-mass stars. In this Letter, we present the first observations of the highly excited NH₃ (3, 3) and (4, 4) lines in this object. Although the presence of highly excited NH₃ in molecular outflows is relatively rare (Bachiller, Martín-Pintado, & Fuente 1993), we have detected shock-heated NH₃ gas and (3, 3) ma-

sers in the jet. By comparing these lines with other tracers, we discuss the driving mechanism of the outflow.

2. OBSERVATIONS

Observations of the NH₃ (J, K) = (3, 3) and (4, 4) inversion transitions were made with the VLA⁴ in the B configuration on 1998 October 8 and in the D configuration on 1999 March 27 and May 29. In all the tracks, we observed both polarizations with a 3.125 MHz bandwidth and 128 channels, yielding a velocity resolution of 0.3 km s⁻¹ at the NH₃ frequencies. The nearby continuum source 2013+370 ($<4^{\circ}$ away) was used as the gain calibrator. The proximity of the two objects is critical to rapid calibrations in the B-array observations, in order to track the atmospheric phase variations. We used a calibration cycle of 110 s with approximately 60 s on the source and 20 s on the calibrator. In the more compact D configuration, a conventional calibration sequence was adopted with a cycle time of about 18 minutes. In all the experiments, the quasar 3C 286 was used as the flux calibrator. The bandpass calibrations were done by observing 3C 273 or 3C 84.

3. RESULTS

Figure 1 presents the integrated emission of the NH₃ (J, K) = (1, 1), (3, 3), and (4, 4) inversion transitions and the SiO J = (2–1) line. In contrast to the extended “core-halo” structure in the NH₃ (1, 1) emission, most of the (3, 3) and (4, 4) emission is found in three discrete clumps, one near the star and two in the outflow region about $10''$ to the northwest and southeast of the star, respectively. The (3, 3) and (4, 4) emission near the star is broadened to greater than 5 km s⁻¹ (FWHM) and is consistent with the warm gas in the rotating disk seen in the (1, 1) and (2, 2) emission (Zhang et al. 1998). The emission also has a component extending to the southeast of the star. Since this component aligns with the axis of the SiO emission (Cesaroni et al. 1999), it is likely to be associated with the jet.

In addition to the emission near the star, the NH₃ (3, 3) and (4, 4) emission is found near the end of the SiO jet. It appears

¹ Harvard-Smithsonian Center for Astrophysics, 60 Garden Street, Cambridge, MA 02138.

² On leave from Raman Research Institute, Bangalore, India.

³ Osservatorio Astronomico di Arcetri, Largo Enrico Fermi 5, Firenze, I-50125, Italy.

⁴ The Very Large Array is a facility of the National Radio Astronomy Observatory, which is operated by Associated Universities, Inc., under contract with the National Science Foundation.

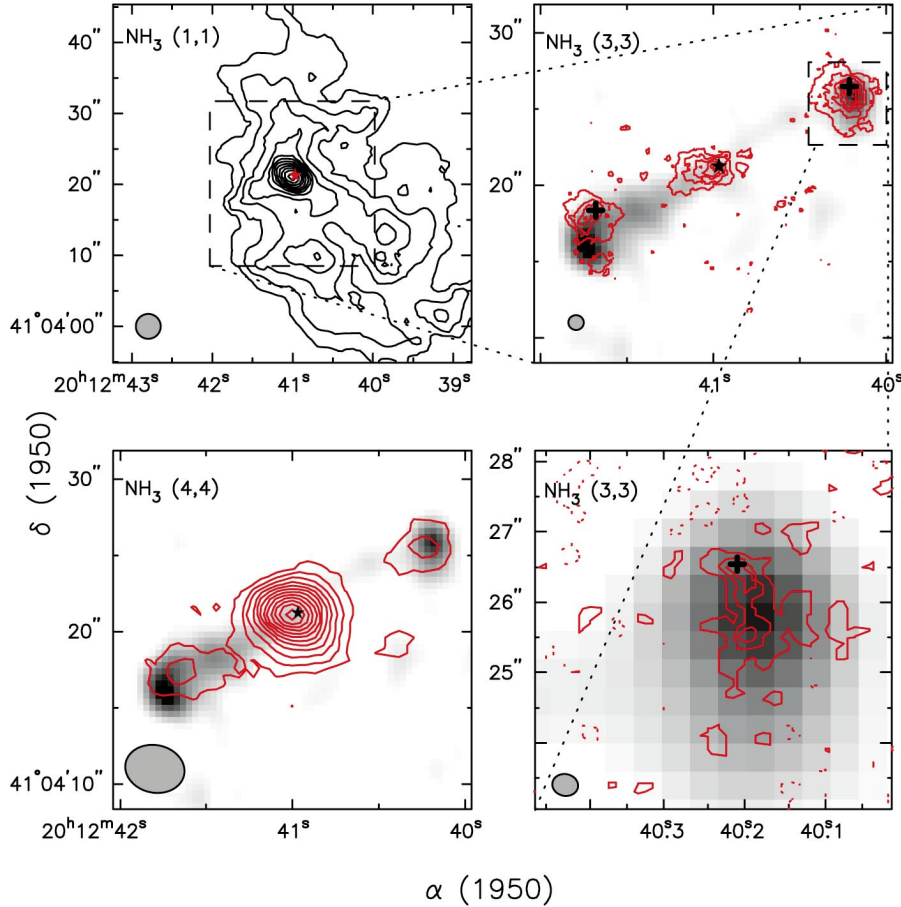


FIG. 1.—NH₃ (3, 3) and (4, 4) emission as compared with the NH₃ (1, 1) emission (Zhang et al. 1998) and the SiO jet (Cesaroni et al. 1999). The NH₃ (1, 1) emission is contoured at every 8% of the peak value of $0.50 \text{ Jy beam}^{-1} (\text{km s}^{-1})$. The NH₃ (3, 3) emission in the upper right panel is made with data from VLA-B and -D arrays with a synthesized beam of $1''$. The emission is integrated from -15 to 10 km s^{-1} and contoured at $(\pm 1, \pm 3, 5, 7, 9, 11) \times 8\%$ of the peak value of $0.23 \text{ Jy beam}^{-1} (\text{km s}^{-1})$. The NH₃ (3, 3) emission in the lower right panel is made with data from VLA-B only with a synthesized beam of $0''.31 \times 0''.37$ at a position angle of 80° . The emission is averaged over -10 to -1 km s^{-1} and contoured at every $3.5 \text{ mJy beam}^{-1}$. The NH₃ (4, 4) emission in the lower left panel is made from VLA-D with a synthesized beam of $3''.9 \times 3''.1$ at a position angle of 78° and is contoured at every 8% of the peak value of $0.34 \text{ Jy beam}^{-1} (\text{km s}^{-1})$. The gray scale for SiO is from 0.1 to $1.5 \text{ Jy beam}^{-1} (\text{km s}^{-1})$. The star marks the position of the 3 mm continuum source, and the shaded ellipse at the lower left-hand corner of each panel denotes the size of the synthesized beam for the NH₃ data. The crosses mark the positions of the NH₃ (3, 3) masers at $\alpha(1950) = 20^{\text{h}}12^{\text{m}}41^{\text{s}}.679 \pm 0^{\text{s}}.001$, $\delta(1950) = 41^{\circ}04'18''.41 \pm 0''.02$ and $\alpha(1950) = 20^{\text{h}}12^{\text{m}}40^{\text{s}}.210 \pm 0^{\text{s}}.001$, $\delta(1950) = 41^{\circ}04'26''.53 \pm 0''.02$.

that the (3, 3) clump to the northwest of the star peaks at the head of the SiO jet and has an arc-shaped structure with the tip farthest from the star. The (3, 3) emission to the southeast of the star is offset $2''$ – $3''$ from the peak of the SiO. The head of the SiO jet delineates a bow, and the NH₃ (3, 3) emission appears in the rear wings of the bow. The (4, 4) emission near each end of the jet is much weaker than the (3, 3) line. It appears that the peak of the (4, 4) emission is offset spatially from the (3, 3) peaks. This offset is more apparent to the southeast of the star where the (4, 4) emission centers closer to the axis of the SiO jet, whereas the (3, 3) emission lies on the sides of the jet.

Figure 2 shows the spectra of the NH₃ (1, 1), (2, 2), (3, 3), and (4, 4) lines at the peak positions in the outflow lobes. Despite the low signal-to-noise ratios in some spectra, it is apparent that all the detected lines are broadened to a few km s^{-1} , in contrast to the 1.6 km s^{-1} FWHM in the quiescent core. In the strongest line (3, 3), the line wings extend to at least $\pm 10 \text{ km s}^{-1}$ (at 3σ) from the core systematic velocity. It is interesting to note that the (3, 3) lines are nearly symmetric

and that the line centers are close to the core systematic velocity. This means that the bulk of the NH₃ gas does not move systematically with respect to the core gas.

For the gas nearest the star, Zhang et al. (1998) derived an optical depth of 2.8 in the (1, 1) main hyperfine component and a rotational temperature of 45 K, consistent with that derived from the (3, 3) and (4, 4) transitions in our present observations. Toward the outflow lobes, assuming that the (1, 1), (2, 2), and (4, 4) lines are optically thin and the NH₃ gas is thermalized, we use the standard rotational diagram to derive the temperature of the gas. We obtain rotational temperatures T_{rot} of 65 and 85 K for the southeast and northwest lobes, respectively. The column density of NH₃ determined from the analysis is 1.4×10^{15} and $1.2 \times 10^{15} \text{ cm}^{-2}$ in the southeast and northwest lobes, respectively.

Compared with the rotational temperature of the NH₃ gas, the (3, 3) emission near each end of the jet has unusually high brightness temperatures. The lower right panel in Figure 1 shows the NH₃ (3, 3) emission at the head of the jet. Even when the emission is averaged between -10 and -1 km s^{-1} ,

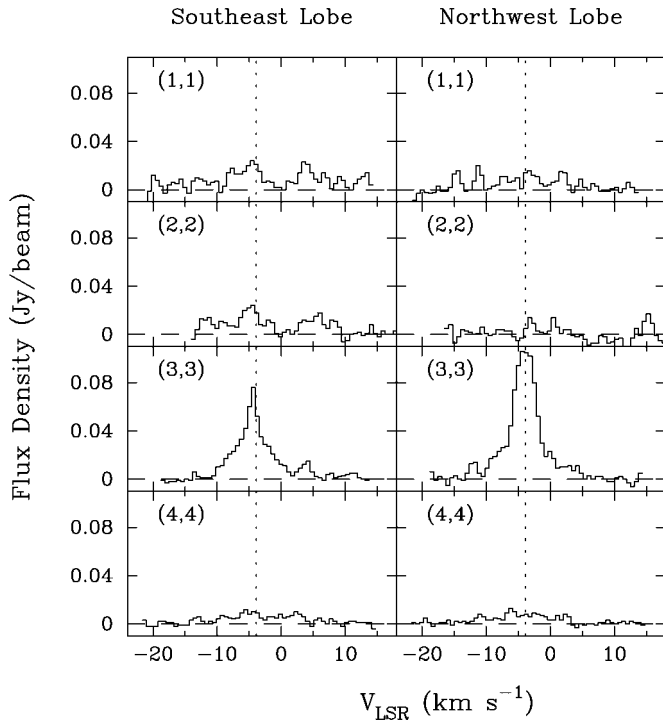


FIG. 2.—Line spectra of the NH_3 (1, 1), (2, 2), and (3, 3) lines from the peak position of NH_3 (3, 3) near the head of the SiO jet. The data are from the VLA-D array with a synthesized beam of about $3''.5$. The vertical dotted line marks the core systematic velocity of -3.7 km s^{-1} .

the highest brightness temperature of the (3, 3) emission⁵ reaches 240 K. The line peaks measured at 0.3 km s^{-1} resolution have typical brightness temperatures that are more than 500 K. The highest brightness temperature arises from two compact spots. Imaged at a resolution of $0''.29 \times 0''.27$, the two features

⁵ The conversion of flux density in units of Jy beam^{-1} to brightness temperature in kelvins follows $\text{K}/(\text{Jy beam}^{-1}) = 120(100 \text{ GHz}/\nu)^2(1''/\theta)^2$, where θ is the angular resolution.

have peak intensities of 79 and 65 mJy beam^{-1} , corresponding to brightness temperatures of 2.2×10^3 and $1.8 \times 10^3 \text{ K}$, respectively. In addition, these features have a narrow line width of 1.5 km s^{-1} in FWHM. The compactness, the narrow line width, and especially the high brightness temperature all indicate maser emission in the NH_3 (3, 3) line.

4. DISCUSSIONS

4.1. Origin of NH_3 Gas in the Outflow

The elevated temperatures ($\geq 65 \text{ K}$) and line broadening of the NH_3 gas in the outflow indicate the heating and energy injection of the gas. The heating provided by a star of $10^4 L_\odot$ to the gas and dust at a distance of 0.086 pc ($10''$) yields an equilibrium temperature of about 25 K. Since this temperature is far less than the observed rotational temperature and since the temperature enhancement is confined only to the jet, the heating of the NH_3 gas is not likely to arise directly from the stellar radiation. It is known that the SiO and H_2 emissions in molecular outflows are by-products of shock activities (Bachiller 1996). The spatial coincidence of the NH_3 and SiO emissions in this object and the arc-like structure in the NH_3 and SiO emissions in the close vicinity of H_2 (Cesaroni et al. 1997) indicate that NH_3 is excited in the bow shock. Such a model is consistent with findings from the CO (7–6) observations (Kawamura et al. 1999) in which the CO gas forms in the trailing regions of the shock.

Although the NH_3 (3, 3) emission shows a good spatial correlation with the high-velocity SiO gas, the profiles of the SiO and NH_3 lines are very different. Figure 3 presents the position-velocity plot of the NH_3 (3, 3) and (4, 4) emission in comparison with the SiO emission from Cesaroni et al. (1999). The SiO emission is detectable at $\pm 50 \text{ km s}^{-1}$ from the cloud velocity and delineates a jet that accelerates with distance from the star. The NH_3 (3, 3) and (4, 4) lines, on the other hand, are limited to a much narrower velocity range of about less than $\pm 10 \text{ km s}^{-1}$.

The difference in kinematics suggests that SiO and NH_3 are produced differently in the shock. The lack of NH_3 emission

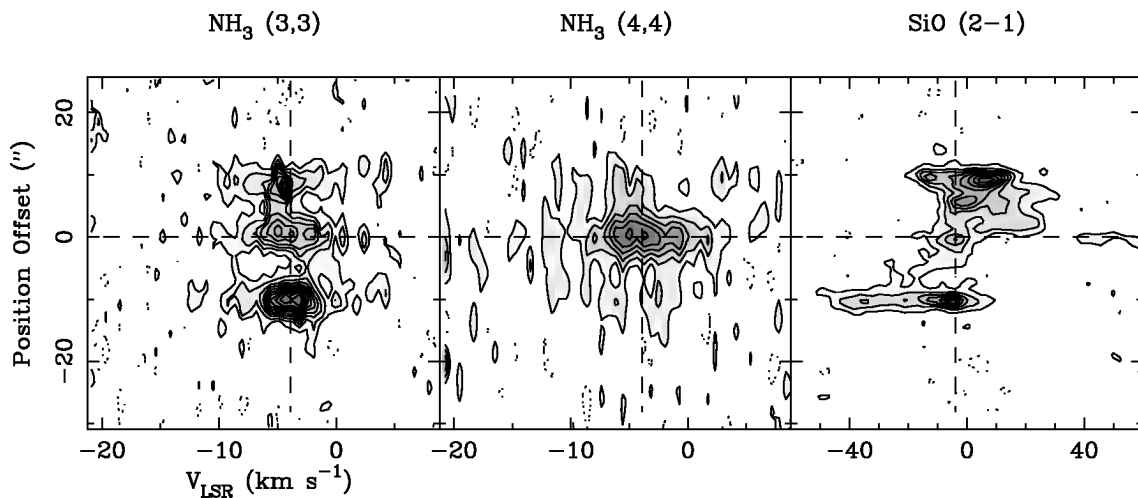


FIG. 3.—Position-velocity plot of the NH_3 (3, 3) and (4, 4) emission in comparison with that of the SiO (2–1) emission. The cut was made at a position angle of 118° along the jet axis with the position offset from the 3 mm continuum source (the star in Fig. 1). The contours for the (3, 3) and (4, 4) emissions are drawn in steps of 10 and 3 mJy beam^{-1} , respectively. The data are from the VLA-D array with a synthesized beam of about $3''.5$. The vertical dashed line marks the core systematic velocity.

at high forward velocities along the jet direction is probably the result of disassociation: The NH₃ molecules are destroyed if the shock velocities are too high. In the extreme case of nonradiative J-type shocks, for instance, the velocity of the postshock gas v_{ps} is $(3/4)v_s$, where v_s is the shock velocity (see Hollenbach 1997). According to Cesaroni et al. (1999), the maximum velocity of the SiO emission, after correcting for the inclination angle, can be as large as 200 km s⁻¹; this implies $v_s > 260$ km s⁻¹. At such velocities, the NH₃ molecules are disassociated in the thin layer of the working surface, and it takes more than 10⁵ yr for them to form (Bergin, Neufeld, & Melnick 1998; E. A. Bergin 1999, private communication). The abundance enhancement of SiO, on the other hand, is more favorable at higher impact velocities because of higher sputtering yield for Si atoms and the relatively short timescales ($\sim 10^2$ yr) for the Si–O reaction (Pineau des Forêts, Flower, & Chièze 1997). It is likely that the observed hot NH₃ lies in the oblique part of the working surface where the shock velocity is low. The lack of NH₃ emission near the southeast tip of SiO supports this scenario. Toward this region, the NH₃ (3, 3) emission appears only toward the rear wings of the bow where the temperatures are likely to be lower than those toward the tip.

In comparison, in the well-studied low-mass outflow L1157, both the NH₃ (3, 3) and SiO lines are skewed to high velocities (Tafalla & Bachiller 1995; Zhang et al. 1995), although the NH₃ line shows far less of the high-velocity wings than the SiO line. A critical difference between the two sources may lie in the shock velocity: The highest velocity of the SiO emission (17 km s⁻¹) in the L1157 outflow suggests a much lower shock velocity than that in the IRAS 20126+4104 outflow. Therefore, NH₃ in L1157 is likely to survive in the working surface and gives rise to the high-velocity wings observed in that object.

4.2. Inversion and Masing of the NH₃ (3, 3) Line

The high brightness temperature (~ 500 K) of the (3, 3) gas near the head of the jet indicates population inversion. For a metastable transition (J, K) of NH₃, the total optical depth is

given by

$$\tau(J, K) = \frac{8\pi^3}{3h} \frac{K^2 \mu^2}{J(J+1)} \frac{2\sqrt{\ln 2}}{\sqrt{\pi}} \Delta v N(J, K) \frac{e^{(hv/kT_{ex})} - 1}{e^{(hv/kT_{ex})} + 1},$$

where $\mu = 1.468$ D, Δv is the FWHM of the line, and $N(J, K)$ is the column density of the transition (see Ho & Townes 1983 and Ungerechts, Winnewisser, & Walmsley 1986). The optical depth is related to the brightness temperature via $T_B = (T_{ex} - 2.7 \text{ K})(1 - e^{-\tau})$. Assuming $N(3, 3) = 10^{15}$ cm⁻² and $\Delta v = 1.5$ km s⁻¹ (see § 3), we find $T_{ex} = -18$ K and $\tau(3, 3) = -3$ for $T_B = 500$ K. Although the actual values may vary depending on the column density, we always obtain negative excitation temperature and optical depth, which are clear indicators of population inversion. The population inversion of the NH₃ (3, 3) emission has been detected toward a number of sources (e.g., W51, Zhang & Ho 1995; NGC 6334, Kraemer & Jackson 1995; DR 21(OH), Mangum & Wootten 1994 and Mauersberger, Wilson, & Henkel 1986). NH₃ (3, 3) inversion can form through collisional excitation of NH₃ by H₂ (Walmsley & Ungerechts 1983) in which the upper level of the NH₃ (3, 3) state exchanges with its (0, 0) state, while the lower level of the (3, 3) state exchanges with the (1, 0) state. Since the transition between the (3, 3)⁺ and (0, 0) states involves a change of parity and thus is more preferred, the (3, 3)⁺ state can be overpopulated.

In conclusion, we observed shock-excited NH₃ (3, 3) emission in the outflow lobes of the young high-mass (proto)star IRAS 20126+4104. The high brightness temperatures (>500 K) of the emission indicate a population inversion in the (3, 3) state. There are two compact features of the NH₃ (3, 3) emission with brightness temperatures exceeding 1800 K. Our observations show that the inversion occurs in the arc-shaped structure near the head of the jet, clearly indicating shock-induced inversion.

This project was partially supported by ASI grant ARS-98-116 to the Osservatorio Astrofisico di Arcetri.

REFERENCES

- Bachiller, R. 1996, *ARA&A*, 34, 111
 Bachiller, R., Martín-Pintado, J., & Fuente, A. 1993, *ApJ*, 417, L45
 Bergin, E. A., Neufeld, D. A., & Melnick, G. J. 1998, *ApJ*, 499, 777
 Cesaroni, R., Felli, M., Jenness, T., Neri, R., Robberto, M., Testi, L., & Walmsley, C. M. 1999, *A&A*, 345, 949
 Cesaroni, R., Felli, M., Testi, L., Walmsley, C. M., & Olmi, L. 1997, *A&A*, 325, 725
 Ho, P. T. P., & Townes, C. H. 1983, *ARA&A*, 21, 239
 Hofner, P., Cesaroni, R., Rodríguez, L. F., & Martí, J. 1999, *A&A*, 345, L43
 Hollenbach, D. 1997, in *Herbig-Haro Flows and the Birth of Low-Mass Stars*, ed. B. Reipurth & C. Dertout (Dordrecht: Kluwer), 181
 Kawamura, J. H., Hunter, T. R., Tong, C.-Y. E., Blundell, R., Zhang, Q., Katz, C., Papa, D. C., & Sridharan, T. K. 1999, *PASP*, 111, 1088
 Kraemer, K. E., & Jackson, J. M. 1995, *ApJ*, 439, L9
 Mangum, J. G., & Wootten, A. 1994, *ApJ*, 428, L33
 Mauersberger, R., Wilson, T. L., & Henkel, C. 1986, *A&A*, 160, L13
 Pineau des Forêts, G., Flower, D. R., & Chièze, J.-P. 1997, in *Herbig-Haro Flows and the Birth of Low-Mass Stars*, ed. B. Reipurth & C. Dertout (Dordrecht: Kluwer), 199
 Tafalla, M., & Bachiller, R. 1995, *ApJ*, 443, L37
 Ungerechts, H., Winnewisser, G., & Walmsley, C. M. 1986, *A&A*, 157, 207
 Walmsley, C. M., & Ungerechts, H. 1983, *A&A*, 122, 164
 Wilking, B. A., Mundy, L. G., Blackwell, J. H., & Howe, J. E. 1989, *ApJ*, 345, 257
 Zhang, Q., & Ho, P. T. P. 1995, *ApJ*, 450, L63
 Zhang, Q., Ho, P. T. P., Wright, M. C. H., & Wilner, D. J. 1995, *ApJ*, 451, L71
 Zhang, Q., Hunter, T. R., & Sridharan, T. K. 1998, *ApJ*, 505, L151